



**HAL**  
open science

## Study of Hydrothermal Stability and Water Sorption Characteristics of 3-Dimensional Zn-Based Trimesate

Tadeja Birsa Čelič, Matjaž Mazaj, Nathalie Guillou, Erik Elkaim, Mohamad El Roz, Frederic Thibault-Starzyk, Gregor Mali, Mojca Rangus, Tomaž Čendak, Venčeslav Kaučič, et al.

► **To cite this version:**

Tadeja Birsa Čelič, Matjaž Mazaj, Nathalie Guillou, Erik Elkaim, Mohamad El Roz, et al.. Study of Hydrothermal Stability and Water Sorption Characteristics of 3-Dimensional Zn-Based Trimesate. Journal of Physical Chemistry C, 2013, 117 (28), pp.14608-14617. 10.1021/jp4036327 . hal-01963791

**HAL Id: hal-01963791**

**<https://hal.science/hal-01963791v1>**

Submitted on 5 Oct 2021

**HAL** is a multi-disciplinary open access archive for the deposit and dissemination of scientific research documents, whether they are published or not. The documents may come from teaching and research institutions in France or abroad, or from public or private research centers.

L'archive ouverte pluridisciplinaire **HAL**, est destinée au dépôt et à la diffusion de documents scientifiques de niveau recherche, publiés ou non, émanant des établissements d'enseignement et de recherche français ou étrangers, des laboratoires publics ou privés.

# Study of hydrothermal stability and water sorption characteristics of 3-dimensional Zn-based trimesate

Tadeja Birsa Čelič,<sup>†</sup> Matjaž Mazaj,<sup>\*,†</sup> Nathalie Guillou,<sup>‡</sup> Erik Elkaïm,<sup>§</sup> Mohamad El Roz,<sup>||</sup> Frederic Thibault-Starzyk,<sup>||</sup> Gregor Mali,<sup>†,⊥</sup> Mojca Rangus,<sup>†</sup> Tomaž Čendak,<sup>†</sup> Vencěslav Kaucič,<sup>†,#</sup> and Natasja Zabukovec Logar<sup>†,#</sup>

<sup>†</sup>National Institute of Chemistry, Hajdrihova 19, 1000 Ljubljana, Slovenia

<sup>‡</sup>Institut Lavoisier, UMR CNRS 8180, Université de Versailles Saint-Quentin-en-Yvelines, 78035 Versailles, France

<sup>§</sup>Soleil Synchrotron, 91192 Gif-sur-Yvette, France

<sup>||</sup>Laboratoire Catalyse et Spectrochimie, ENSICAEN, Université de Caen, CNRS, 6 Bd Maréchal Juin, F-14050 Caen, France

<sup>°</sup>EN-FIST Centre of Excellence, Dunajska 156, 1000 Ljubljana, Slovenia

<sup>⊥</sup>CO-NOT Centre of Excellence, Hajdrihova 19, 1000 Ljubljana, Slovenia

To be submitted to The Journal of Physical Chemistry C

April 2013

**KEYWORDS.** Metal-organic frameworks, hydrothermal stability, zinc trimesate, water sorption, MAS NMR spectroscopy

**ABSTRACT.** A zinc trimesate  $Zn_2(BTC)(OH)(H_2O) \cdot 1,67H_2O$  with the three-dimensional framework contains  $[Zn_2O_6(OH)_2(H_2O)]$  chains with the arrangement of  $ZnO_2(OH)_2$  tetrahedra and  $ZnO_4(OH)(H_2O)$  octahedra corner-shared through  $\mu_3$ -OH group. Inorganic chains are linked with 1,3,5-benzenetricarboxylates forming two types of parallel channels (open and closed) containing adsorbed water in different environments. Closed channels are occupied by free water molecules connected through strong hydrogen-bonds with coordinated water, whereas open-type channels contain water molecules with partially occupied oxygen atom sites. The dynamics of water adsorption/desorption was well evaluated by complementary techniques of TG, IR, water sorption and different MAS NMR techniques. The removal of water from open channels occurs below 100 °C, whereas hydrogen-bonded water molecules and coordinated water are expelled at higher temperatures.  $^2H$  MAS NMR was employed to prove that the removal of water from closed channels is not entirely simultaneous and that adsorbed water begins to diffuse at slightly lower temperatures than the coordinated one. The investigated material shows high hydrothermal and withstands 40 cycle-hydrothermal stability tests without any significant loss of structure integrity. It also shows complete structural reversibility upon dehydration/rehydration process at 200 °C. The reason for high chemical resistivity to water mainly lies in the presence of the adsorbed water molecules interacting with the coordinated ones (framework water) by hydrogen bonds. The material also exhibits notable sorption capacity for water (208 mg·g<sup>-1</sup>) adsorbed in stepwise process.

**INTRODUCTION.** The rational design of porous metal-organic frameworks (MOFs) aiming for the production of materials with the desired applicative properties is currently one of the most active research areas in the field of crystal engineering.<sup>1-8</sup> The development of MOFs is

particularly focused for separation, catalysis and gas storage applications, due to their well-defined pore architectures, high surface areas, low framework densities and high concentration of active sites represented by free metal sites or organic functional groups. Great potential for the above mentioned applications that this group of materials offers is in large extent limited by their un-stability in humid conditions.<sup>9-15</sup> Knowledge of MOF performance under humid conditions is crucial before elevating these materials to the applied level. However, the parameters that contribute to the sensitivity to water are still relatively poorly understood.<sup>16-20</sup> It was already shown that pyrazolates and imidazolates in general exhibit higher chemical resistivity to water than carboxylate-based MOFs. Which is related to higher basicity ( $pK_a$ ) of the nitrogen-based ligand and consequently stronger metal-ligand bonds in comparison with oxygen-based carboxylate ligands.<sup>16,17,20-24</sup> Despite the fact that carboxylate-based MOFs tend to exhibit lower structure stability in water than pyrazolate or imidazolates, there are quite a few MOF carboxylates that withstand exposure to water even at elevated temperatures without significant losses of their structure integrities. The most frequently investigated water-resistant MOF members are MIL-53(Al, Cr), MIL-101(Cr), MIL-100(Cr), UiO-66(Zr) and MIL-125(Ti).<sup>25-29</sup> This exceptions suggest that structure stability in water is not only governed by the basicity of the ligand and thus the strength of the metal-ligand bond but it is related to many other independent factors such as metal type, coordination state and framework dimensionality.<sup>20,30,31</sup>

MOFs with good hydrothermal stability and specific structural properties such as high specific surface areas, high affinities and adsorption capacities for water and possibility to tune the hydrophilic nature of their frameworks during the synthesis are appropriate candidates for water sorption based energy applications (heat storage, heat pumps processes). Although possibilities of MOFs for water sorption applications are still relatively unexplored, several MOF systems were already examined for this purpose: DUT-4(Al)<sup>13</sup>, MOF-74(Mg)<sup>17</sup>,

UiO-66(Zr)<sup>17</sup>, DMOF-1(Zn)<sup>17</sup>, UMCM-1(Zn)<sup>17</sup>, MIL-101(Cr)<sup>32-36</sup>, MIL-100(Fe)<sup>32,33</sup>, MIL-53(Al)<sup>33</sup>, HKUST-1(Cu)<sup>33</sup>, ISE-1(Ni)<sup>33</sup> and ZIF-8(Zn)<sup>33</sup>. Among these materials MIL-101(Cr) shows the best performance for heat transfer applications. It exhibits high hydrothermal stability, huge water sorption uptakes up to 1.4 g·g<sup>-1</sup> of sorbent at 25 °C and high desorption rates below 80 °C. On the other hand Zn-based carboxylates (DMOF-1, UMCM-1, IRMOFs) undergo significant loss of crystallinity upon water exposure, therefore they are in general evaluated to be unsuitable for such applications.<sup>14,17,20,23</sup>

In the present study we report on the solvothermal synthesis of a Zn-trimesate, Zn<sub>2</sub>(BTC)(OH)(H<sub>2</sub>O)·1,67H<sub>2</sub>O material containing tetrahedrally and octahedrally coordinated Zn centres which are connected through BTC linkers to the extended 3-dimensional structure with two types of parallel channels.<sup>37</sup> We showed that material exhibits an exceptional hydrothermal stability, complete reversibility upon dehydration-rehydration process and notable water sorption capacity. The reason for high hydrothermal stability mainly lies in the stabilization of inorganic chains by hydrogen-bonded water molecules, which was evaluated by complementary techniques of solid state NMR, XRD, *in-situ* IR and water sorption measurements. High water resistance even at elevated temperatures, which is a rare feature among Zn-based MOFs, together with promising water sorption properties implies that investigated Zn-trimesate is a potential material for water sorption based energy applications.

## EXPERIMENTAL SECTION

**Synthesis.** For the synthesis of Zn<sub>2</sub>(BTC)(OH)(H<sub>2</sub>O)·1,67H<sub>2</sub>O we modified the procedure published by Fu et al.<sup>37</sup> Solvothermal synthesis was performed under autogenous pressure from a mixture of zinc acetate dehydrate (98 % Zn(CH<sub>3</sub>CO<sub>2</sub>)<sub>2</sub>·2H<sub>2</sub>O, Aldrich), 1,3,5-benzentricarboxylic acid (95 % BTC, Aldrich), ethanol (99.8 %, Aldrich) and distilled water. The molar ratios of starting reagents were Zn(ac)<sub>2</sub>·2H<sub>2</sub>O : BTC : 100 H<sub>2</sub>O : 70 EtOH. Zinc

acetate was dissolved in distilled water and an ethanolic solution of trimesic acid was prepared separately. White gel obtained immediately after solutions were combined was stirred for 5 minutes, transferred into Teflon-lined stainless-steel 25 mL autoclave and treated at 175 °C for 24 hours. White crystalline powder was thoroughly rinsed with ethanol and/or water and dried at room temperature. The comparison of the measured powder X-ray diffractogram with the calculated one confirmed that the material contained pure  $\text{Zn}_2(\text{BTC})(\text{OH})(\text{H}_2\text{O}) \cdot 1,67\text{H}_2\text{O}$  phase (see Supporting Information).<sup>37</sup>

**General characterization methods and sorption measurements.** Thermogravimetric (TG/DTG) analysis was performed on a SDT 2960 Thermal Analysis System (TA Instruments, Inc.). The measurement was carried out in static air with the heating rate of 10 °C/min. Thermal stability was monitored by high-temperature XRD measurements in vacuum employing a PANalytical X'Pert PRO MPD diffractometer from 5 to 55°  $2\theta$  using step of 0.013° per 100 s in the temperature range between 25 and 700 °C. Structural changes and hydrothermal stability were monitored by powder X-ray diffraction measurements on a PANalytical X'Pert PRO high-resolution diffractometer with Alpha1 configuration ( $\text{CuK}\alpha_1$   $\lambda = 1.5406 \text{ \AA}$  radiation) using continuous scanning mode in  $2\theta$  range from 5 to 35° with the step of 0.016° per 100 s.

$^1\text{H}$  (Magic-Angle Spinning) and  $^1\text{H}$ - $^{13}\text{C}$  CPMAS (Cross-Polarization Magic-Angle Spinning) NMR spectra were recorded on a 600 MHz Varian NMR system equipped with a 3.2 mm Varian probehead. Larmor frequencies for  $^1\text{H}$  and  $^{13}\text{C}$  were 599.72 MHz and 150.82 MHz, sample rotation frequencies were 20 kHz and 16 kHz, and the numbers of scans were 64 and 600, respectively. Repetition delays between scans were 5 s in all experiments.  $^1\text{H}$  90° excitation pulse was 2  $\mu\text{s}$ .  $^1\text{H}$ - $^{13}\text{C}$  CPMAS experiment employed RAMP<sup>38</sup> during CP block and high-power XiX<sup>39</sup> heteronuclear decoupling during acquisition. Chemical shifts of  $^1\text{H}$  and

$^{13}\text{C}$  signals were referenced to the corresponding signals of tetramethylsilane. Variable-temperature  $^2\text{H}$  MAS NMR spectra were acquired on the same spectrometer using a 5 mm Doty probehead and sample rotation frequency of 12 kHz.  $^2\text{H}$  Larmor frequency was 92.05 MHz,  $90^\circ$  excitation pulse was 6  $\mu\text{s}$ , repetition delay was 5 s and number of scans was 128. Before the  $^2\text{H}$  NMR measurements the sample was evacuated at 200  $^\circ\text{C}$  for two hours and subsequently a drop of  $^2\text{H}_2\text{O}$  was added to it. Variable-temperature NMR measurement started when the drop was completely absorbed.

For *in-situ* infrared spectroscopy powders were pressed ( $\sim 10^7$  Pa) into self-supported discs (2  $\text{cm}^2$  area, 9-11  $\text{mg cm}^{-2}$ ). They were placed in a cell equipped with KBr windows. A movable quartz sample holder allowed placing the pellet in the infrared beam for recording spectra and moving it into a furnace at the top of the cell for thermal treatment. The cell was connected to a vacuum line for evacuation ( $P \sim 10^{-5}$  torr), and a gauge controls the pressure of the vapors of  $\text{H}_2\text{O}$  (or  $\text{D}_2\text{O}$ ) introduced into the cell. A Nicolet 6700 IR spectrometer equipped with a MCT detector and an extended-KBr beam splitter was used for the acquisition of spectra recorded in the 400-5500  $\text{cm}^{-1}$  range. Spectra were recorded at 4  $\text{cm}^{-1}$  and 128 scans were co-added for each spectrum.

Water sorption characteristics of Zn-trimesate were determined by an IGA-100 gravimetric analyzer (Hiden Isochema Ltd). Water sorption isotherms were obtained at 30  $^\circ\text{C}$  by setting equal pressure intervals of 1.6 mbar between vacuum and 40 mbar (saturation vapor pressure of 42.5 mbar at 30  $^\circ\text{C}$ ) with an equilibrium time of 80 s. Before adsorption measurements, the sample was outgassed to a constant weight under ultra high vacuum ( $<10^{-5}$  mbar) at 200  $^\circ\text{C}$  for three hours. The hydrothermal stability of the material was additionally evaluated with cycle test measurements consisting of 40 cycles between designated temperatures of 40 and 140  $^\circ\text{C}$  in a helium gas flow with 75 % relative humidity. The relative humidity was controlled by varying the ratio of dry and saturated helium via two mass flow controllers.

## RESULTS AND DISCUSSION

### Structure description, thermal properties and water removal studies.

$\text{Zn}_2(\text{BTC})(\text{OH})(\text{H}_2\text{O}) \cdot 1,67\text{H}_2\text{O}$  consists of one-dimensional chains which are composed of  $\text{ZnO}_2(\text{OH})_2$  tetrahedral and  $\text{ZnO}_4(\text{OH})(\text{H}_2\text{O})$  octahedral units connected through corner-shared  $\mu_3$ -hydroxy bridging groups. (Figure 1 left). Octahedral and tetrahedral entities are additionally linked by carboxylate groups of BTC moieties. In this way the  $[\text{Zn}_2\text{O}_6(\text{OH})(\text{H}_2\text{O})]_n$  chains are connected into the extended three-dimensional structure with two types of parallel channels which can be denoted as closed and opened channels (Figure 1 right). Closed channels are occupied by water molecules (Ow1) coordinated to octahedral Zn atoms and have no available free space. The opened channels with the free space diameter of 5 Å contain adsorbed water molecules on partially occupied sites Ow3 and Ow4. There is another water molecule (Ow2, full occupancy) located between the Ow1 vertices of two nearby  $\text{ZnO}_4(\text{OH})(\text{H}_2\text{O})$  octahedra (Figure 1 left). This water molecule interacts with the Zn-coordinated water through hydrogen bonds (Ow1...Ow2 distance of 2.794(13) Å).

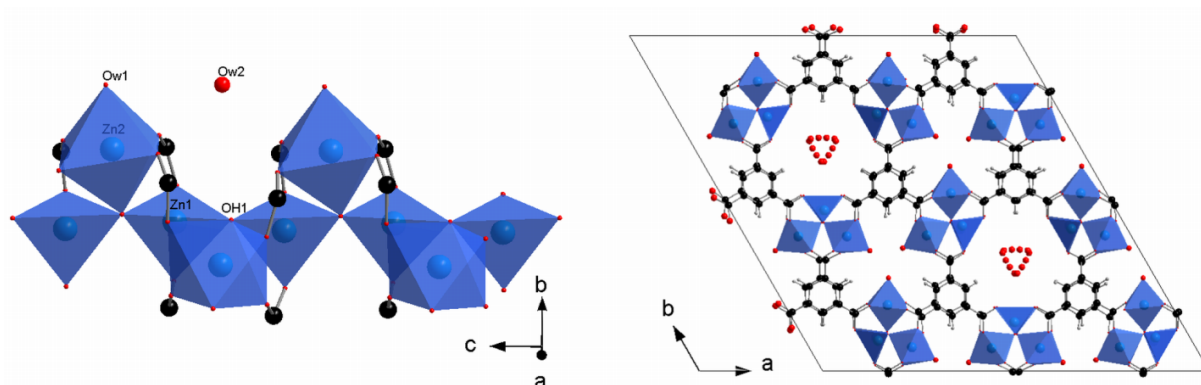


**Figure 1.** Polyhedral presentation of 1-dimensional  $[\text{Zn}_2\text{O}_6(\text{OH})_2(\text{H}_2\text{O})]_n$  chain with carbon atoms belonging to carboxylate groups and oxygen atom belonging to water molecule (Ow2). The chain is running along c-axis bridged through carboxylate groups (left). A view of

$\text{Zn}_2(\text{BTC})(\text{OH})(\text{H}_2\text{O})\cdot 1,67\text{H}_2\text{O}$  structure along *c*-direction with the unit cell edges revealing closed and opened types of channels. Opened channels contain water molecules with partially occupied oxygen atoms sites (Ow3, Ow4) (right). Blue circles – zinc atoms, red dots and circles – oxygen atoms, black circles – carbon atoms, grey circles – hydrogen atoms.

As it will be described later in the text, it was found that in this study investigated Zn-trimesate exhibit high hydrothermal stability and the arrangement of water moieties within the framework seems to be one of the key factors which contributes to the chemical resistivity towards water of this material. Thermogravimetric analysis was already briefly described by Fu et al.<sup>37</sup>, however to gain more knowledge about the type and the location of water molecules within the structure, TG analysis was performed again and additionally supported by the detailed *in-situ* IR and NMR discussions. The thermogravimetric (TG/DTG) curves (Figure 2) shows that  $\text{Zn}_2(\text{BTC})(\text{OH})(\text{H}_2\text{O})\cdot 1,67\text{H}_2\text{O}$  loses weight in three steps. In the first step the loss of approximately 3 wt. % of the total mass could be attributed to the release of adsorbed water located within the open channels. The detected loss corresponds to the removal of 0.7 water molecules (Ow3, Ow4) per one asymmetric unit. Removal of adsorbed water at temperatures below 100 °C can be explained by the fact that the open channels have a relatively hydrophobic nature and are big enough for unobstructed and easy water diffusion from the material. The second step with the weight loss of 9.1 wt.% could be attributed to the simultaneous desorption of the remaining hydrogen-bonded water molecules (Ow2) located within the closed channels and the coordinated water molecules (Ow1). Both water molecules fully occupy their crystallographic positions and theoretically the removal of these water moieties would correspond to the loss of 9.0 wt.% of the total mass. The reason for the delayed release of the water located on the Ow2 sites compared to the water molecules adsorbed within the open channels can be explained by the presence of the above mentioned

strong hydrogen bonding and also by the fact that these water molecules are located within narrower channels from which the diffusion is expected to be slower. Weight loss of 3.1 wt.% in the third step could be attributed to the removal of  $\mu_3$ -bridging OH groups. Since the theoretical weight loss for the removal of these groups is bigger (4.3 wt.%) than the measured one, we can conclude that OH groups are not completely removed in the temperature range between 250 and 350 °C within the 10 minutes time period (heating ramp = 10 °C/min). Removal of the remaining OH groups takes place during the final framework decomposition.

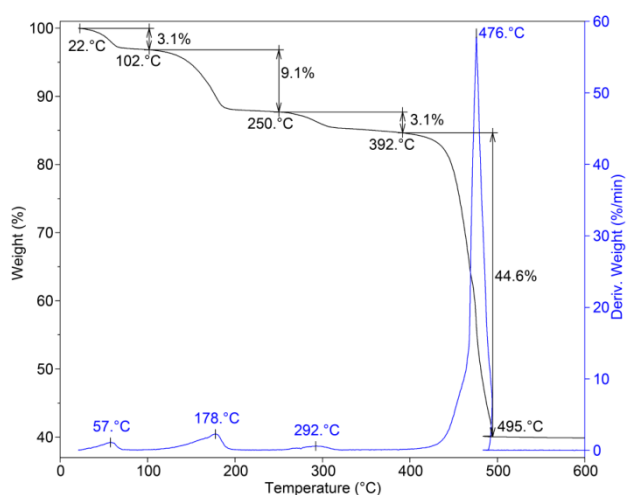


**Figure 2.** Thermogravimetric analysis of  $\text{Zn}_2(\text{BTC})(\text{OH})(\text{H}_2\text{O}) \cdot 1,67\text{H}_2\text{O}$  material. TG - black curve, DTG – blue curve.

In order to support the above proposed arrangement of water molecules, *in-situ* IR measurements were performed. The complexity of the IR profile depends on the hydroxylation degree of the surface. Figure 3 shows the comparison of IR spectra of  $\text{Zn}_2(\text{BTC})(\text{OH})(\text{H}_2\text{O}) \cdot 1,67\text{H}_2\text{O}$  recorded at ambient conditions and after heating at 200 °C. The broad IR-bands at  $5380\text{-}4820\text{ cm}^{-1}$  and  $3762\text{-}2644\text{ cm}^{-1}$  are assigned to the free water molecules within the pores and coordinated water to Zn atoms (Ow1), respectively.<sup>40,41</sup> After activation, the IR bands assigned to  $\text{H}_2\text{O}$  disappeared in comparison with the original IR

spectrum indicating that physisorbed and coordinated water are totally removed from the material.

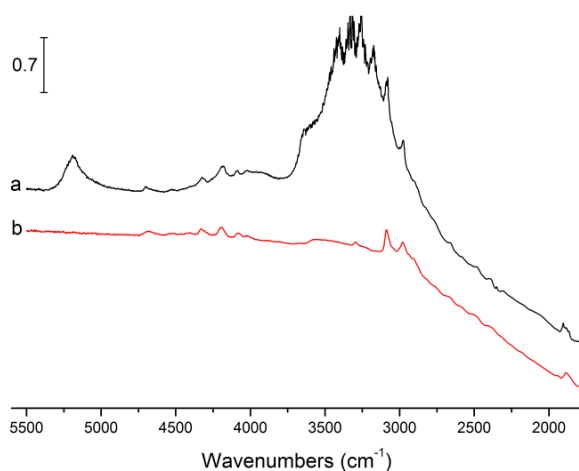


**Figure 3.** IR spectra of Zn-trimesate under air (a) and after activation at 200°C under vacuum for 2 hours (b).

$^1\text{H}$  and  $^2\text{H}$  MAS NMR spectroscopy put an additional light on the information about environment of water molecules and the dynamics of its removal from the  $\text{Zn}_2(\text{BTC})(\text{OH})(\text{H}_2\text{O})\cdot 1,67\text{H}_2\text{O}$  material.  $^1\text{H}$  MAS spectra of the as-prepared material and of the materials thermally treated (*ex-situ*) at 100 °C, 200 °C and 300 °C are shown in Figure 4a. In the spectrum of the as-prepared Zn-trimesate we can distinguish three contributions at approximately 7.7 ppm, 4.4 ppm and 1.6 ppm. The three signals can be assigned to the hydrogen atoms in the benzene ring, in the water molecules, and in the hydroxyl groups, respectively. Thermal treatment of the material at 100 °C and 200 °C reduces the intensity of the 4.4 ppm peak, but hardly affects the intensities of the 7.7 and 1.6 ppm peaks. The latter peak is suppressed only when the sample is heated to 300 °C. These thermally induced changes, firstly, confirm the assignments of the 4.4 ppm peak to water molecules and the 1.6 ppm peak to hydroxyl groups, and secondly, support the observations of the thermal analysis, showing that water molecules are largely expelled from the pores of the Zn-trimesate up to the

temperature of about 250 °C. It is interesting to note that the 4.4 ppm  $^1\text{H}$  NMR signal becomes asymmetric when the material is heated to 100 °C, suggesting that the signal is actually composed of more than one contribution. Since the intensity of the water signal at 100 °C is already reduced as compared to the intensity of the water signal of the as-prepared sample and since it is proposed that water molecules from the open channels are already desorbed at this temperature, the asymmetry of the 4.4 ppm  $^1\text{H}$  NMR signal indicates that water molecules that are coordinated to Zn atoms and water molecules that are hydrogen bonded to the framework resonate at slightly different chemical shifts. When the sample is further heated to 200 °C, the  $^1\text{H}$  NMR signal of the water molecules is still lowered and apparently shifted to smaller isotropic chemical shift, confirming that one of the contributions to the  $^1\text{H}$  NMR signal of water molecules was removed. It seems that the removal of the hydrogen-bonded water molecules and the removal of the coordinated water molecules, which according to the thermal analysis both take place in the temperature interval between approximately 100 °C and 200 °C, are not entirely simultaneous and that most probably slightly higher temperatures are needed to completely expel the coordinated water molecules from the closed channels. At 300 °C the signal of the hydroxyl groups reduces significantly and the signal belonging to water molecules finally becomes negligible.

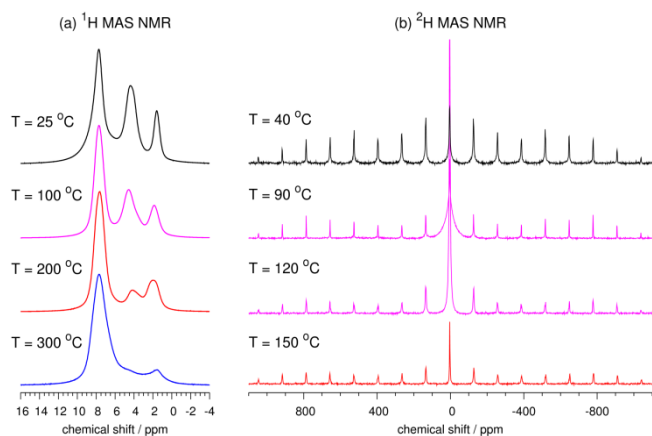


**Figure 4.**  $^1\text{H}$  (a) and  $^2\text{H}$  (b) MAS NMR spectra of  $\text{Zn}_2(\text{BTC})(\text{OH})(\text{H}_2\text{O})\cdot 1,67\text{H}_2\text{O}$ . Thermal treatment of the sample for the  $^1\text{H}$  MAS NMR measurement was performed *ex-situ* and thermal treatment of the sample for the  $^2\text{H}$  MAS NMR was carried out *in-situ* within the NMR probe.

Complementary information on the removal of water and on its dynamics is offered by the *in-situ* variable-temperature  $^2\text{H}$  MAS NMR spectroscopy of the sample in which  $^1\text{H}_2\text{O}$  molecules were replaced by  $^2\text{H}_2\text{O}$  (heavy water) molecules. The  $^2\text{H}$  spectra recorded at 40 °C, 90 °C, 120 °C and 150 °C are shown in Figure 4b. Note that the listed temperatures correspond to the temperatures reported by the sensor within the NMR probehead and do not match exactly the temperatures as observed in the thermal analysis or as used for the *ex-situ* treatment of the sample. All  $^2\text{H}$  MAS NMR spectra exhibit typical broad spinning-sideband powder patterns, which are due to the strong anisotropic interaction of  $^2\text{H}$  nuclei with the local electric-field gradients. The increasing temperature causes several changes in the spectra. When the temperature is increased from 40 °C to 90 °C the shape of the spinning-sideband powder pattern changes significantly, the overall intensity of the sideband pattern reduces and the central peak at about 4 ppm substantially broadens. The resulting spectrum can be described as a sum of two contributions; one for which the sideband pattern composed of narrow signals can be well fitted by a quadrupole pattern with CQ of 140 kHz, and another which exhibits only a broad central peak at about 4 ppm. Since at the temperature of 90 °C water molecules that were located within the open channels are already expelled from the sample, the two contributions must belong to the coordinated and the hydrogen-bonded water molecules. The different appearance of the two contributions reflects the very different dynamics of the two types of water. The broad quadrupolar sideband pattern corresponds to water molecules exhibiting relatively slow dynamics and can thus be assigned to the coordinated water molecules. Differently, the broad single central peak could belong to water

molecules that undergo intermediately fast dynamic processes, because of which the quadrupolar sideband pattern gets reduced and thus limited to the central peak only (and perhaps to few weak sidebands that cannot be resolved because of their large linewidth) and because of which the centreband (and individual sidebands) get 'motionally broadened'.<sup>42</sup> This observation suggests that upon heating the sample from 40 °C to 90 °C the dynamics of the previously hydrogen-bonded water molecules become notably faster and that the hydrogen bonds between them most probably break apart. When the temperature is further increased to 120 °C the 'free' water molecules enter the fast dynamics regime; the centreband and the first-rank sidebands become 'motionally narrowed'<sup>42</sup>, while the quadrupolar sideband pattern gets significantly reduced. The shape of the broad quadrupolar pattern belonging to the coordinated water molecules does not change, but its intensity drops slightly. Heating the sample to 150 °C drastically reduces the intensity of the central peak, showing that most of the uncoordinated water gets removed from the pores. The signal of the water coordinated to zinc is still present but lowered even further. This means that also the coordinated water molecules are being expelled from the material, but the temperature for this process needs to be higher or the thermal treatment needs to last longer than for the removal of the hydrogen-bonded molecules.

The location of water moieties and their dynamics during the heating process was well evaluated and the next step was to monitor structural changes of the framework during the thermal treatment. The changes were monitored *in-situ* by high-temperature XRD and *ex-situ* by <sup>1</sup>H-<sup>13</sup>C CPMAS NMR and the obtained diffraction patterns and spectra are shown in Figure 5. We can see that the removal of adsorbed water from the open channels (up to 75 °C) does not affect the framework structure. Structural changes begin to occur only above 100 °C, when the processes of remaining water desorption from the closed channels and removal of coordinated water start. Changes in peak positions in the temperature range between 100 and

150 °C indicate a certain degree of framework flexibility, which is required if the framework is to withstand the removal of the coordinated water. Most of the peaks at higher angles are broadened and significantly lowered due to the anisotropic effects or structural defects that may occur during the thermal treatment.

The second structural change caused by the removal of the  $\mu_3$ -bridging OH groups begins at 250 °C. Bridging OH groups connect the  $\text{ZnO}_2(\text{OH})_2$  and  $\text{ZnO}_4(\text{OH})(\text{H}_2\text{O})$  polyhedra into the inorganic chain, and their removal causes the collapse or reorganization of the chains and leads to the substantial decrease in crystal structure ordering. In the temperature range between 400 and 500 °C the framework of Zn-trimesate finally decomposes and transforms to wurtzite ZnO phase.

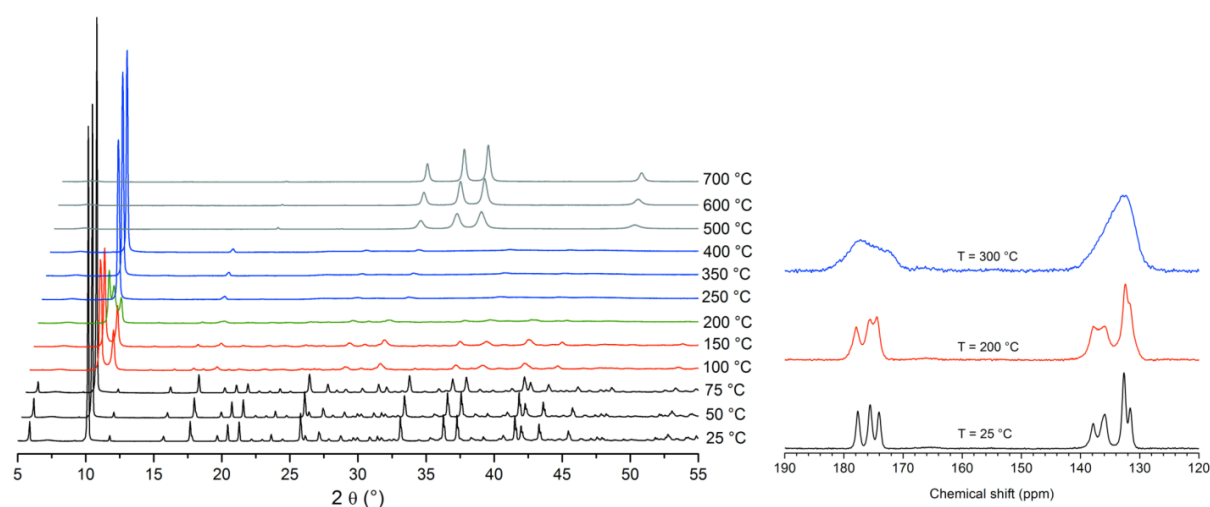


**Figure 5.** HT-XRD patterns of  $\text{Zn}_2(\text{BTC})(\text{OH})(\text{H}_2\text{O}) \cdot 1.67\text{H}_2\text{O}$  thermally treated at given temperatures measured in vacuum (left) and  $^1\text{H}$ - $^{13}\text{C}$  CPMAS NMR spectra of the material treated ex-situ at selected temperatures (right).

Very similar information can be deduced also from the  $^1\text{H}$ - $^{13}\text{C}$  CPMAS NMR spectra (Figure 5). The spectrum of the as-prepared material exhibits very narrow signals indicating

that the material is very well crystalline. The contributions of the three crystallographically distinct carboxyl carbon atoms are clearly resolved one from another, and also the carbon nuclei within the benzene ring detect slightly different local environments and resonate at slightly different frequencies. Heating the sample up to 200 °C only slightly changes the  $^1\text{H}$ - $^{13}\text{C}$  CPMAS spectrum. The individual signals become somewhat broader and therefore start to overlap one another more intensely, yet all the above-described contributions can still be distinguished. The signal positions do not change because of the thermal treatment at 200 °C, showing that the organic part of the framework is practically unaffected by the removal of water molecules.  $^1\text{H}$ - $^{13}\text{C}$  CPMAS spectrum changes drastically only when the sample is heated to 300 °C. At this temperature the signals in the NMR spectrum get severely broadened and thus indicate that the framework becomes significantly less ordered.

**Stability in water and water sorption properties.** The fact that the framework of the  $\text{Zn}_2(\text{BTC})(\text{OH})(\text{H}_2\text{O})\cdot 1,67\text{H}_2\text{O}$  is very little affected by the removal of water suggests that the material could be efficiently rehydrated. Indeed, as shown by the *in-situ* variable-temperature XRD measurements in air flow in Figure 6, the dehydration–rehydration process is completely reversible if the material is exposed to air for more than one hour. The reversibility of the process is confirmed also by the comparison of the  $^1\text{H}$ - $^{13}\text{C}$  CPMAS NMR spectra recorded before and after the dehydration-rehydration cycle (inset in Figure 6). Furthermore, the Zn-trimesate material is hydrothermally stable and its structure can withstand different water treatment procedures - water adsorption, treatment in boiling water, hydrothermal cycling from 40 to 140 °C at constant humidity and water adsorption after cycling procedure. As can be seen in Figure 7, it is apparent that any kind of water exposure procedure does not affect the crystal structure significantly. These XRD patterns will be discussed in more details later in the text.

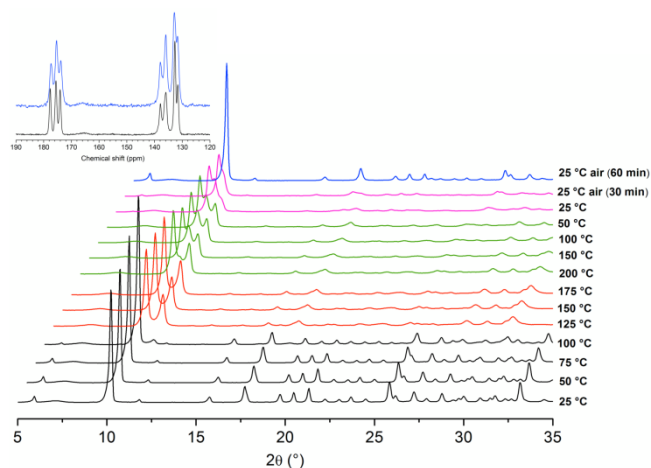


**Figure 6.** HT-XRD patterns of Zn-trimesate during the heating up to 200 °C and cooling down to ambient temperature and additionally exposed to air for different periods of time. Inset shows  $^1\text{H}$ - $^{13}\text{C}$  CPMAS NMR spectra of the material recorded before and after the dehydration-rehydration cycle.

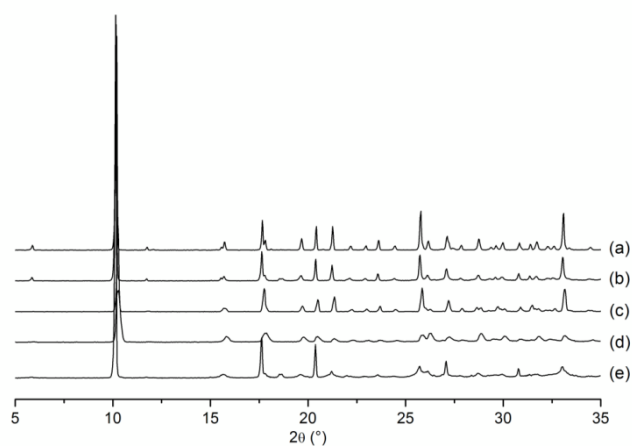


**Figure 7.** XRD patterns of as-synthesized material (a), after water sorption isotherm (b), after treatment in boiling water for 18 h (c), after 40 cycles (d) and after 40 cycles and water sorption isotherm (e).

The removal of adsorbed water from open channels should yield microporous framework with one-dimensional parallel channels with the diameter of 5 Å. Therefore it is expected that pores of the activated material are accessible for gas molecules. However, sorption

measurements with different gases ( $N_2$ ,  $CO_2$ ,  $H_2$ ) on degassed Zn-trimesate did not show any notable uptakes. On the other hand, the material exhibits better uptakes for water. The water adsorption isotherm recorded at 30 °C on Zn-trimesate is shown in Figure 8. The maximum water uptake is 208 mg per gram of material at a relative pressure  $p/p_0$  of 0.95. It is apparent that the shape of the water adsorption isotherm is of type I in the IUPAC classification scheme, indicating that the investigated material has hydrophilic character and that interactions between water and the framework are strong. In the lower pressure range from  $p/p_0 = 0.02 - 0.3$  stepwise water adsorption can be observed indicating the presence of two energetically different processes. Firstly, water molecule coordinates to the free zinc metal sites via coordination bonds since Zn-trimesate contain open-metal site after heating the sample at 200 °C. Interestingly, similar adsorption on the available metal sites in the lower pressure region of adsorption process was previously reported for HKUST-1 and MIL-100(Al, Fe, Cr) type compound.<sup>12,43,44</sup> Additional filling of the pores on hydrophilic sites takes place and finally also remaining open channels are filled with water molecules. In the higher pressure region above  $p/p_0 = 0.9$ , additional adsorption occurs which is the result of condensation of water in pores. Although the adsorption and desorption branches are quite similar, the hysteresis can be observed. The notable hysteresis in the low pressure region indicates that some water molecules are very strongly bonded to the framework of  $Zn_2(BTC)(OH)(H_2O) \cdot 1,67H_2O$ .

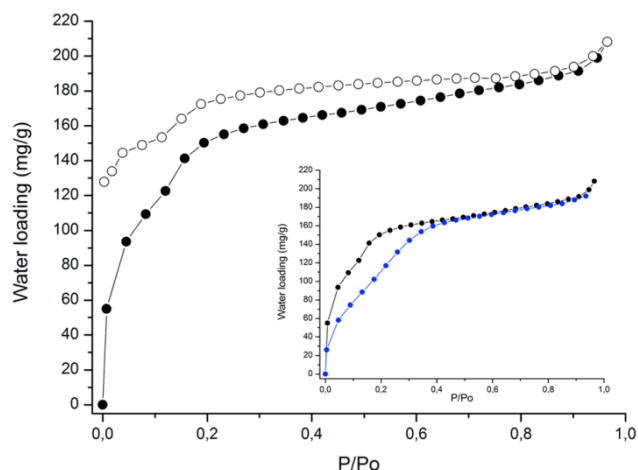


**Figure 8.** H<sub>2</sub>O vapor adsorption and desorption isotherms for degassed Zn-trimesate (black filled circles – absorption; black empty circles – desorption). Inset shows adsorption isotherms before (black circles) and after hydrothermal cycling (blue circles) measured at 30 °C.

The isosteric heat of adsorption,  $q_{st}$  was estimated by applying Dubinin-Raduschevich equation<sup>45</sup> using the sorption data at 30 °C. Heat of adsorption values were calculated in different relative pressure ranges of the isotherm (Supporting information Figure S2, Table S4). At very low relative pressure the isosteric heat value is high (~57 kJ·mol<sup>-1</sup>) since the sample is dry and energetically favorable metal sites are free to be occupied. In the following adsorption steps the value slowly decreases to approximately 47 kJ·mol<sup>-1</sup>, which is very close to the molar evaporation enthalpy of water at 30 °C (~ 44 kJ·mol<sup>-1</sup>). The trend obtained and the isosteric values are comparable with those previously reported.<sup>43,44</sup>

The adsorption of water into activated Zn-trimesate was also investigated by IR. An *in-situ* IR study has been performed by introducing small amounts of water to the dried sample (rehydration process). The results are presented in Figure 9. The introduction of water causes the reappearance and progressive increase of the IR bands at 5235 cm<sup>-1</sup> and 3615 cm<sup>-1</sup> which

were disappeared after activation (Figure 9 a). Figure 9 b presents the evolution of the combination band area ( $\nu+\delta(\text{H}_2\text{O})$ ) at  $5235\text{ cm}^{-1}$  and the intensity of the IR band at  $3615\text{ cm}^{-1}$  as a function of the amount of introduced water. For the amount of water lower than  $2.5\text{ }\mu\text{mol}$ , an increase of the  $\nu(\text{OH})$  bands of the coordinated water at  $3615\text{ cm}^{-1}$  is observed. This is not the case for the  $\nu+\delta(\text{H}_2\text{O})$  band at  $5235\text{ cm}^{-1}$  which slowly increases for  $2.5 < n(\text{H}_2\text{O}) < 10\text{ }\mu\text{mol}$  and starts to increase more rapidly for  $n(\text{H}_2\text{O}) > 10\text{ }\mu\text{mol}$ . It is accompanied with an increase of the broad IR band at  $3315\text{ cm}^{-1}$  assigned to the vibration modes of hydrogen-bonded physisorbed water molecules. These results show that water molecules are adsorbed preferentially on the free metal sites and the excess of water is stoked in the channels as physisorbed water.

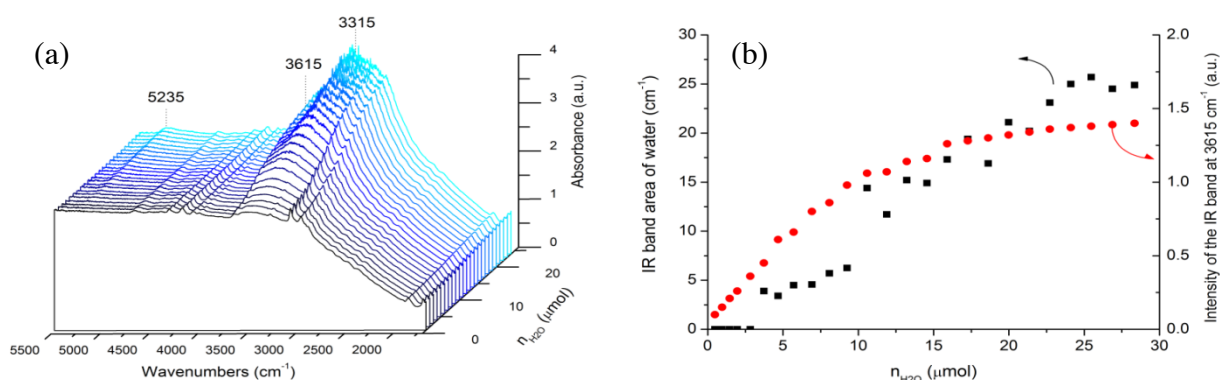


**Figure 9.** (a) Evolution of the IR spectra of activated Zn-trimesate during the water adsorption. (b) Dependence of the combination band area and intensity of the coordinated water IR band at  $3615\text{ cm}^{-1}$  with the amount of the adsorbed water in  $\mu\text{mol}$ .

Since it was proved that  $\text{Zn}_2(\text{BTC})(\text{OH})(\text{H}_2\text{O})\cdot 1,67\text{H}_2\text{O}$  material shows a good chemical stability towards water, it was also analyzed under continuous hydro-thermal cycling ( $40\text{-}140\text{ }^\circ\text{C}$ ,  $75\%$  relative humidity) in order to estimate its stability and potential suitability for water sorption applications<sup>33</sup>. From obtained results of a durability test

(Supporting Information Figure S3), it can be seen that the water loading capacity is reduced by 20 % in comparison to the initial uptake after 20 cycles but remains almost unchanged after 40 cycles. Although, the slight loss of water sorption capacity evidently occurs during the 40 cycles experiment,  $\text{Zn}_2(\text{BTC})(\text{OH})(\text{H}_2\text{O}) \cdot 1,67\text{H}_2\text{O}$  still shows higher stability in water than almost all zinc MOFs and also some other MOF materials (MOF-5, MOF-69, HKUST-1).<sup>9,12,20</sup> The comparison of water adsorption isotherms (inset in Figure 8) of Zn-trimesate phase before and after the hydrothermal cycling treatment indicate that the adsorption capacity for water at high relative pressures remains the same after the hydrothermal cycling treatment under humid conditions. However in the low relative pressure region the water adsorption process is slower than in the initial material. Adsorption is still stepwise but the steps are much less pronounced. Interestingly, even though the inflection point between two steps is shifted towards higher  $p/p_0$  values (0.1 and 0.2 before and after hydrothermal cycling treatment, respectively), it occurs at approximately the same water loading amounts (cca.  $120 \text{ mg} \cdot \text{g}^{-1}$ ). At relative pressure of 0.4 the water loading reaches saturation and adsorption branch above  $p/p_0 = 0.4$  becomes comparable with the isotherm of Zn-trimesate before cycling treatment. The slower adsorption processes of the material after hydrothermal cycling in both steps at low pressure range can be explained by slight structural changes which may occur during the long-term hydrothermal cycling treatment. The framework changes can cause partial blocking of the 1-dimensional channels which means that adsorption sites become more obstructed and less accessible for water molecules. Thus higher pressures or longer time are needed for water to coordinate back to Zn(II) cations. Partial structural changes are indicated by XRD pattern analysis of the sample after cycling treatment where the peaks are broadened and slightly shifted toward higher angles (Figure 7 d) if compared with the XRD pattern of the sample after first isotherm measurement (Figure 7 b). At relative pressures between 0.4 and 1.0, where water capacity reaches the values of the original (degassed as-

synthesized) sample, the Zn-trimesate framework seems to be completely recovered. The assumption of structure recovering can be again supported by XRD analysis. XRD pattern of the sample measured after hydrothermal cycling and subsequent water isotherm treatment shows sharpening of the peaks, increasing of intensities and shifting back towards lower angles (Figure 7 e). We can conclude that even though the long-term hydrothermal cycling between 40 and 140 °C at constant humidity slightly affects the Zn-trimesate framework and its water loading capacity, the structure of this material can be completely recovered by exposure to humid conditions at ambient temperatures.

### THE CONCLUSIONS CAN ALSO START HERE...

Hydrothermal stability of metal-organic frameworks is in most cases dependent on the ability to exchange organic ligand moieties with water molecules or affinity to hydrolysis. In order to understand chemical resistivity towards water for the  $\text{Zn}_2(\text{BTC})(\text{OH})(\text{H}_2\text{O}) \cdot 1,67\text{H}_2\text{O}$ , some typical MOF features which can govern above mentioned chemical processes should be discussed in more details. 1) Type of the connection node between metal and electron donor group. Ligands which are bonded to metal cations in  $\eta^2$  fashion can be displaced more easily and thus allow easier ligand-to-water exchange, than those connected in  $\eta^1$  node. Consequently, MOFs with  $\eta^1$  ligand-to-metal connection type are expected to be more stable than MOFs with  $\eta^2$  type of connection. 2) Coordination number and oxidation state of metal cation. Metal cations possessing larger coordination numbers (eg. octahedral) tend to be more stable than those with lower ones (eg. tetrahedral). Tetrahedral geometry provides more available space for additional water molecule to coordinate to metal which can lead to hydrolysis. Higher oxidation state of metal cations or metal clusters should also lead to higher relative stability towards water reaction. 3) Geometry of secondary building units (SBUs). Dimensionality of the metal-containing SBU and its connectivity in MOF structure is another

important factor which affects stability in water. 1-D chain-like SBUs tend to contribute to higher water resistance of the MOFs than 0-D clusters. However, in the case of structures with 1-D SBUs, the type of connections of the individual polyhedra to chain-like units is the factor that should also be considered. Edge-sharing polyhedral SBUs are more robust and seem to exhibit relatively higher water resistance than less rigid SBUs with corner-shared polyhedra.

4) Metal-oxygen bond strength. Stronger interactions between metal cation and oxygen atoms should obviously contribute to higher hydrothermal stability of the framework, since ligand displacement or exchange with water is expected to be less favorable as in the structures with weaker metal-oxygen bonds.<sup>9,14,20,41,46,47</sup>

Taking into account all the structural features described in the previous paragraph, relatively high water resistance of  $\text{Zn}_2(\text{BTC})(\text{OH})(\text{H}_2\text{O})\cdot 1,67\text{H}_2\text{O}$  can be explained by several structural features that this framework possesses. Firstly, the structure is composed of tetrahedral and octahedral Zn-centered chains, where stability in water media should be indeed higher than in the presence of 0-dimensional cluster SBUs. Secondly, polyhedra are bridged through  $\eta^1$  carboxylate nodes, thus the ligand displacement process is not as favorable as in the case of  $\eta^2$  carboxylate node configuration. 50 % of all Zn atoms are in octahedral environment which also may have some contribution to the higher stability in water. The benzene rings stacked along *c*-axis at the average distance of 3.47 Å forms  $\pi$ - $\pi$  interactions which additionally stabilizes the framework.<sup>48</sup> The last and in our opinion most pronounced feature which contributes to the water stability is the presence of the hydrogen-bonded water interacting with the framework (coordinated) water molecules. As it was clearly shown by NMR and HT-XRD analyses the dehydrated material (heated at 200 °C) is completely recovered back to  $\text{Zn}_2(\text{BTC})(\text{OH})(\text{H}_2\text{O})\cdot 1,67\text{H}_2\text{O}$  material upon exposure to the moisture. Additional investigations by water sorption measurements indicated that hydrogen-bonded water molecules occupy their positions first with relatively high heat of adsorption values (>

57 kJ·mol<sup>-1</sup>). Dehydrated material obviously has high tendency to adsorb hydrogen-bonded water molecules (Ow2) to interact with the framework (coordinated) water. This plays a key role in the stabilization of inorganic chains and increases the chemical stability in hydrothermal conditions. The exceptional hydrothermal stability is a rarity in Zn-based MOF materials. Relatively high stability in water has been reported for imidazolate framework (ZIF-8), but to our knowledge the investigated material is beside MOF-74, which possesses chains of Zn octahedra, the only carboxylate-based Zn-MOF to exhibit such properties.<sup>47,49</sup>

CONCLUSION. We presented the studies of water stability and water sorption behavior of 3-dimensional Zn-trimesate material  $\text{Zn}_2(\text{BTC})(\text{OH})(\text{H}_2\text{O}) \cdot 1,67\text{H}_2\text{O}$ . Structure contains inorganic SBU, described as  $[\text{Zn}_2\text{O}_6(\text{OH})(\text{H}_2\text{O})]_n$ , and composed of  $\text{ZnO}_2(\text{OH})_2$  tetrahedra and  $\text{ZnO}_4(\text{OH})(\text{H}_2\text{O})$  octahedra which are corner-shared through  $\mu_3\text{-OH}$  group. Chains are connected through BTC linkers forming two types of parallel channels which contain adsorbed water in different environments. Dynamic of water adsorption/desorption was thoroughly investigated by TG, IR, water sorption and different MAS NMR techniques. <sup>2</sup>H MAS NMR elucidated the sequence of removal of coordinated water and hydrogen-bonded water molecules, whereas those processes could not be resolved by TG analysis. Thus, the <sup>2</sup>H MAS NMR turned out to be a useful technique for distinguishing the dynamics of molecular species during the heating process, where those species occur in similar chemical environment.  $\text{Zn}_2(\text{BTC})(\text{OH})(\text{H}_2\text{O}) \cdot 1,67\text{H}_2\text{O}$  show surprisingly high hydrothermal stability for Zn-based MOFs since it is not significantly affected by water exposure even after 40-cycle hydrothermal treatment and shows structural reversibility upon dehydration/rehydration process up to 200 °C. We showed that adsorbed water molecules interacting with coordinated (framework) water by hydrogen bonds play a key role in stabilizing the framework structure and in large extent contribute to the high stability of the material in water. The material also

shows notable water adsorption capacity. Exceptional stability in water is a rarity for Zn-based MOFs and to our knowledge  $\text{Zn}_2(\text{BTC})(\text{OH})(\text{H}_2\text{O})\cdot 1,67\text{H}_2\text{O}$  represents the only zinc-based carboxylate beside MOF-74 to exhibit such properties. Further developments of isorecticular materials with hydrothermal stability comparable to this Zn-trimesate can be achieved by using bulkier tridentate ligands and could expand the applicability of MOFs for water sorption-based storage applications.

## ASSOCIATED CONTENT

**Supporting Information.** Calculated and measured XRD patterns, scanning electron micrograph of Zn trimesate crystals,  $\text{N}_2$  adsorption isotherm, DR plots and hydrothermal cycle test. This material is available free of charge via the Internet at <http://pubs.acs.org>.

## AUTHOR INFORMATION

### Corresponding Author

\* Email: [matjaz.mazaj@ki.si](mailto:matjaz.mazaj@ki.si). Phone: +38614760215. Fax.: +38614760300

### Notes

The authors declare no competing financial interest.

## ACKNOWLEDGMENT

This work was supported by the Slovenian Research Agency research programme P1-0021 and BI-FR/11-12-PROTEUS-011 project.

## ABBREVIATIONS

MOFs, metal-organic frameworks; SBU, secondary building unit; BTC, 1,3,5-benzenetricarboxylic acid; NMR, nuclear magnetic resonance; ICP-AES, inductively coupled

plasma atomic emission spectrometer; XRD, X-Ray diffraction; CPMAS, cross-polarization magic angle spinning; TG, Thermogravimetric analysis; DTG, Derivative Thermogravimetric analysis; ZIF, zeolitic imidazolate framework; HKUST, Hong Kong University of Science and Technology; MIL, Materials of Institut Lavoisier.

## REFERENCES

- (1) Li, H.; Eddaoudi, M.; O’Keeffe, M.; Yaghi, O.M. Design and Synthesis of an Exceptionally Stable and Highly Porous Metal-Organic Framework. *Nature* **1999**, *402*, 276-279.
- (2) Kitaura, R.; Iwahori, F.; Matsuda, R.; Kitagawa, S.; Kubota, Y.; Takata, M.; Kobayashi, T.C. Rational Design and Crystal Structure Determination of a 3-D Metal–Organic Jungle-Gym-like Open Framework. *Inorg. Chem.* **2004**, *43*, 6522-6524.
- (3) Li, C.-J.; Hu, S.; Li, W.; Lam, C.-K.; Zheng, Y.-Z.; Tong, M.-L. Rational design and control of the dimensions of channels in three-dimensional porous metal-organic frameworks constructed with predesigned hexagonal layers and pillars. *Eur. J. Inorg. Chem.* **2006**, *10*, 1931-1935.
- (4) Marchal, C.; Filinchuk, Y.; Imbert, D.; Bünzli, J.-C. G.; Mazzanti, M. Towards the Rational Design of Lanthanide Coordination Polymers: A New Topological Approach. *Inorg. Chem.* **2007**, *46*, 6242-6244.
- (5) Xie, Y.; Yu, Z.; Huang, X.; Wang, Z.; Niu, L.; Teng, M.; Li, J. Rational Design of MOFs Constructed from Modified Aromatic Amino Acids. *Chem. Eur. J.* **2007**, *13*, 9399-9405.

- (6) Xue, M.; Zhu, G.; Zhang, Y.; Fang, Q.; Hewitt, I.J.; Qiu, S. Rational Design and Control of the Dimensions of Channels in a Series of 3D Pillared Metal–Organic Frameworks: Synthesis, Structures, Adsorption, and Luminescence Properties. *Cryst. Growth Design* 2008, 8, 427-434.
- (7) Sadakiyo, M.; Yamada, T.; Kitagawa, H. Rational Designs for Highly Proton-Conductive Metal-Organic Frameworks. *J. Am. Chem. Soc.* **2009**, 131, 9906-9907.
- (8) Farha, O.K.; Malliakas, C.D.; Kanatzidis, M.G.; Hupp, J.T. Control over Catenation in Metal-Organic Frameworks via Rational Design of the Organic Building Block. *J. Am. Chem. Soc.* **2010**, 132, 950-952.
- (9) Greathouse, J. A.; Allendorf, M. D. The Interaction of Water with MOF-5 Simulated by Molecular Dynamics. *J. Am. Chem. Soc.* **2006**, 128, 10678-10679.
- (10) Kondo, A.; Daimaru, T.; Noguchi, H.; Ohba, T.; Kaneko, K.; Kanoh, H. Adsorption of water on three-dimensional pillared-layer metal organic frameworks. *J. Colloid Interface Sci.* **2007**, 314, 422-426.
- (11) Castillo, J. M.; Vlugt, T. J. H.; Calero, S. Understanding Water Adsorption in Cu–BTC Metal–Organic Frameworks. *J. Phys. Lett. C* **2008**, 112, 15934-15939.
- (12) Küsgens, P.; Rose, M.; Senkovska, I.; Fröde, H.; Henschel, A.; Siegle, S.; Kaskel, S. Characterization of metal-organic frameworks by water adsorption. *Microporous Mesoporous Mater.* **2009**, 120, 325-330.
- (13) Paranthaman, S.; Coudert, F.-X.; Fuchs, A. H. Water adsorption in hydrophobic MOF channels. *Phys. Chem. Chem. Phys.* **2010**, 12, 8123-8129.

(14) Cychoosz, K. A.; Matzger, A. J. Water Stability of Microporous Coordination Polymers and the Adsorption of Pharmaceuticals from Water. *Langmuir* **2010**, *26*(22), 17198-17202.

(15) Hauptvogel, I. M.; Biedermann, R.; Klein, N.; Senkovska, I.; Cadiau, A.; Wallacher, D.; Feyerherm, R.; Kaskel, S. Flexible and Hydrophobic Zn-Based Metal–Organic Framework. *Inorg. Chem.* **2011**, *50*, 8367-8374.

(16) Liang, Z.; Marshall, M.; Chaffee, A.L. CO<sub>2</sub> Adsorption, Selectivity and Water Tolerance of Pillared-Layer Organic Frameworks. *Microporous Mesoporous Mater.* **2010**, *132*, 305-310.

(17) Schoenecker, P.M.; Carson, C.G.; Jasuja, H.; Flemming, C.J.J. Effect of Water Adsorption on Retention of Structure and Surface Area of Metal-Organic Frameworks. *Ind. Eng. Chem. Res.* **2012**, *51*, 6513-6519.

(18) Jasuja, H.; Burch, N.C.; Huang, Y.; Cai, Y.; Walton, K.S. Kinetic Water Stability of an Isostructural Family of Zinc-Based Pillared Metal-Organic Frameworks. *Langmuir* **2013**, *29*, 633-642.

(19) Han, S.; Huang, Y.; Watanabe, T.; Nair, S.; Walton, K.S.; Sholl, D.S.; Meredith, J.C. MOF Stability and Gas Adsorption as a Function of Exposure to Water, Humid Air, SO<sub>2</sub>, and NO<sub>2</sub>. *Microporous Mesoporous Mater.* **2013**, *173*, 86-91.

(20) Low, J.J.; Benin, A.I.; Jakubczak, P.; Abrahamian, J.F.; Faheem, S.A.; Willis, R.R. Virtual High Throughput Screening Confirmed Experimentally: Porous Coordination Polymer Hydration. *J. Am. Chem. Soc.* **2009**, *131*, 15834-15842.

(21) Choi, H.J.; Dinca, M.; Dailly, A.; Long, J.R. Hydrogen Storage in Water-Stable Metal-Organic Frameworks Incorporating 1,3- and 1,4-Benzenedipyrazolate. *Energy Environ. Sci.* **2010**, *3*, 117-123.

(22) Colombo, V.; Galli, S.; Choi, H.J.; Han, G.D.; Maspero, A.; Palmisano, G.; Masciocchi, N.; Long, J.R. High Thermal and Chemical Stability in Pyrazolate-Bridged Metal-Organic Frameworks with Exposed Metal Sites. *Chem. Sci.* **2011**, *2*, 1311-1319.

(23) Li, Y.; Yang, R.T. Gas Adsorption and Storage in Metal-Organic Framework MOF-177. *Langmuir* **2007**, *23*, 12937-12944.

(24) Kaye, S. S.; Dailly, A.; Yaghi, O. M.; Long, J. R. Impact of preparation and handling on the hydrogen storage properties of  $Zn_4O(1,4\text{-benzenedicarboxylate})_3$  (MOF-5). *J. Am. Chem. Soc.* **2007**, *129*, 14176-14177.

(25) Serre, C.; Millange, F.; Thouvenot, C.; Noguès, M., Marsolier, G, Louër, D.; Férey, G. Very Large Breathing Effect in the First Nanoporous Chromium(III)-Based Solids: MIL-53 or  $Cr^{III}(OH)\cdot\{O_2C-C_6H_4-CO_2\}_x\cdot\{HO_2C-C_6H_4-CO_2H\}_x\cdot H_2O_y$ . *J. Am. Chem. Soc.* **2002**, *124*, 13519-13526.

(26) Loiseau, T.; Serre, C.; Huguenard, C.; Fink, G.; Taulelle, F.; Henry, M.; Bataille, T.; Férey, G. A Rationale for the Large Breathing of the Porous Aluminum Terephthalate (MIL-53) Upon Hydration. *Chem. Eur. J.* **2004**, *10*, 1373-1382.

(27) Férey, G.; Serre, C.; Mellot-Draznieks, C.; Millange, F.; Soublié, S.; Dutour, J.; Margiolaki, I. A Hybrid Solid with Giant Pores Prepared by a Combination of Targeted Chemistry, Simulation, and Powder Diffraction. *Angew. Chem. Int. Ed.* **2004**, *43*, 6296-6301.

(28) Cavka, J.H.; Jakobsen, S.; Olsbye, U.; Guillou, N.; Lamberti, C.; Bordiga, S.; Lillerud, K.P. A New Zirconium Inorganic Building Brick Forming Metal Organic Frameworks with Exceptional Stability. *J. Am. Chem. Soc.* **2008**, *130*, 13850-13851.

(29) Dan-Gardi, M.; Serre, C.; Frot, T.; Rozes, L.; Maurin, G.; Sanchez, C.; Férey, G. A New Photoactive Crystalline Highly Porous Titanium(IV) Dicarboxylate. *J. Am. Chem. Soc.* **2009**, *131*, 10857-10859.

(30) Kang, I. J.; Khan, N. A.; Haque, E.; Jhung, S. H.; Chemical and Thermal Stability of Isotypic Metal-Organic Frameworks: Effect of Metal Ions. *Chem. Eur. J.* **2011**, *17*, 6437-6442.

(31) Ma, D.; Li, Y.; Li, Z. Tuning the Moisture Stability of Metal-Organic Frameworks by Incorporating Hydrophobic Functional Groups at Different Positions of Ligands. *Chem. Commun.* **2011**, *47*, 7377-7379.

(32) Seo, Y.-K.; Yoon, J. W.; Lee, J. S.; Hwang, Y. K.; Jun, C.-H.; Chang, J.-S.; Wuttke, S.; Bazin, P.; Vimont, A.; Daturi, M.; Bourelly, S.; Llewellyn, P. L.; Horcajada, P.; Serre, C.; Férey, G. Energy-Efficient Dehumidification over Hierarchically Porous Metal-Organic Frameworks as Advanced Water Adsorbents. *Adv. Mater.* **2012**, *24*, 806-810.

(33) Henninger, S.K.; Jeremias, F.; Kummer, H.; Janiak, C. MOFs for Use in Adsorption Heat Pump Processes. *Eur. J. Inorg. Chem.* **2012**, 2625-2634.

(34) Ehrenmann, J.; Henninger, S. K.; Janiak, C. Water Adsorption Characteristics of MIL-101 for Heat-Transformation Applications of MOFs. *Eur. J. Inorg. Chem.* **2011**, 471-474.

(35) Khutia, A.; Rammelberg, H.U.; Schmidt, T.; Henninger, S.; Janiak, C. Water Sorption Cycle Measurements on Functionalized MIL-101Cr for Heat Transformation Application. *Chem. Mater.* **2013**, *25*, 790-798.

(36) Akiyama, G.; Matsuda, R.; Sato, H.; Hori, A.; Takata, M.; Kitagawa, S. Effect of Functional Groups in MIL-101 on Water Sorption Behavior. *Microporous Mesoporous Mater.* **2012**, *157*, 89-93.

(37) Fu, Y.; Li, G.; Liao, F.; Xiong, M.; Lin, J. Two Novel Transition Metal-Organic Frameworks Based on 1,3,5-Benzenetricarboxylate Ligand: Syntheses, Structures and Thermal Properties. *J. Mol. Struct.* **2011**, *1004*, 252-256.

(38) Metz, G.; Wu, X.; Smith, S. O. Ramped-Amplitude Cross Polarization in Magic-Angle-Spinning NMR. *J. Magn. Reson. A* **1994**, *110*, 219-227.

(39) Detken, A.; Hardy, E.H.; Ernst, M.; Meier, B.H. Simple and efficient decoupling in magic-angle spinning solid-state NMR: the XiX scheme. *Chem. Phys. Lett.* **2002**, *356*, 298-304.

(40) Vimont A.; Goupil, J.-M.; Lavalley J.-C.; Daturi, M., Surble, S.; Serré, C.; Millange, F.; Férey, G.; Audebrand, N. Investigation of Acid Sites in a Zeotypic Giant Pores Chromium(III) Carboxylate. *J. Am. Chem. Soc.* **2006**, *128*, 3218-3227.

(41) Tan, K.; Nijem, N.; Canepa, P.; Gong Q.; Li, J.; Thonhauser, T.; Chabal, Y. J. Stability and Hydrolyzation of Metal Organic Frameworks with Paddle-Wheel SBUs upon Hydration. *Chem. Mater.* **2012**, *24*, 3153-3167.

(42) Kristensen, J. H.; Hoatson, G. L.; Vold, R. L. Investigation of multiaxial molecular dynamics by  $^2\text{H}$  MAS NMR spectroscopy. *Solid State Nucl. Magn. Reson.* 1998, *13*, 1-37.

(43) Akiyama, G.; Matsuda, R.; Kitagawa, S. Highly Porous and Stable Coordination Polymers as Water Sorption Materials. *Chem. Lett.* **2010**, *39*, 360-361.

(44) Jeremias, F.; Khutia, A.; Henninger, S. K.; Janiak, C. MIL-100(Al, Fe) as water adsorbents for heat transformation purposes - a promising application. *J. Mater. Chem.* **2012**, *22*, 10148-10151.

(45) Dubinin, M. M. The potential theory of adsorption of gases and vapors for adsorbents with energetically nonuniform surfaces. *Chem. Rev.* **1960**, *39*, 235-241.

(46) Davies, K.; Bourne, S.A.; Ohrstrom, L.; Oliver, C.L. Anionic zinc-trimesic acid MOFs with unusual topologies: reversible hydration studies. *Dalton Trans.* **2010**, *39*, 2869-2874.

(47) Park, K. S.; Ni, Z.; Côté, A. P.; Choi, J. Y.; Huang, R.; Uribe-Romo, F. J.; Chae, H. K.; O'Keeffe, M.; Yaghi, O. M. Exceptional chemical and thermal stability of zeolitic imidazolate frameworks. *Proc. Natl. Acad. Sci. U.S.A.* **2006**, *103*, 10186-10191.

(48) Kostakis, G.E.; Casella, L.; Hadjiliadis, N.; Monzani, E.; Kourkoumelis, N.; Plakatouras, J.C. Interpenetrated networks from a novel nanometer-sized pseudopeptidic ligand, bridging water, and transition metal ions with cds topology. *Chem. Commun.* **2005**, 3859-3861.

(49) Rosi, N.L.; Kim, J.; Eddaoudi, M.; Chen, B.; O'Keeffe, M.; Yaghi, O.M. Rod Packings and Metal–Organic Frameworks Constructed from Rod-Shaped Secondary Building Units. *J. Am. Chem. Soc.* **2005**, *127*, 1504-1518.